LETTER

A graphene–based broadband optical modulator

Ming Liu[1]*, Xiaobo Yin[1]*, Erick Ulin-Avila[1], Baisong Geng[2], Thomas Zentgraf[1], Long Ju[2], Feng Wang[2,3] & Xiang Zhang[1,3]

Integrated optical modulators with high modulation speed, small footprint and large optical bandwidth are poised to be the enabling devices for on-chip optical interconnects[1,2]. Semiconductor modulators have therefore been heavily researched over the past few years. However, the device footprint of silicon-based modulators is of the order of millimetres, owing to its weak electro-optical properties[3]. Germanium and compound semiconductors, on the other hand, face the major challenge of integration with existing silicon electronics and photonics platforms[4–6]. Integrating silicon modulators with high-quality-factor optical resonators increases the modulation strength, but these devices suffer from intrinsic narrow bandwidth and require sophisticated optical design; they also have stringent fabrication requirements and limited temperature tolerances[7]. Finding a complementary metal-oxide-semiconductor (CMOS)-compatible material with adequate modulation speed and strength has therefore become a task of not only scientific interest, but also industrial importance. Here we experimentally demonstrate a broadband, high-speed, waveguide-integrated electroabsorption modulator based on monolayer graphene. By electrically tuning the Fermi level of the graphene sheet, we demonstrate modulation of the guided light at frequencies over 1 GHz, together with a broad operation spectrum that ranges from 1.35 to 1.6 μm under ambient conditions. The high modulation efficiency of graphene results in an active device area of merely 25 μm^2, which is among the smallest to date. This graphene-based optical modulation mechanism, with combined advantages of compact footprint, low operation voltage and ultrafast modulation speed across a broad range of wavelengths, can enable novel architectures for on-chip optical communications.

Graphene, a single sheet of carbon atoms in a hexagonal lattice, has attracted great interest because of its exceptional electrical and optical properties[8–13]. Graphene couples strongly to light, which enables observation of monolayer graphene under an optical microscope with the naked eye. A pristine graphene monolayer has a constant absorption of $\pi\alpha = 2.3\%$ across the infrared and visible range, where α is the fine-structure constant ($e^2/\hbar c$, where e is the electronic charge, $\hbar$ is Planck's constant divided by 2π, and c the velocity of light). Moreover, the broad optical absorption in graphene can be controlled through electrical gating: by shifting the electronic Fermi level, one can controllably change graphene's optical transitions[14,15]. The strong electroabsorption effect, which has not yet been observed in bulk materials, originates from graphene's unique electronic structure and its two-dimensional character. It implies that graphene has the potential to be used as the active medium in an optical electroabsorption modulator. However, one of the challenges involved in a direct graphene modulator is the limited absorption of a monolayer. This can be overcome by integrating graphene with an optical waveguide, which greatly increases the interaction length through the coupling between the evanescent waves and graphene.

A graphene-based waveguide-integrated electroabsorption modulator has several distinctive advantages. (1) Strong light–graphene interaction. In comparison to compound semiconductors, such as those exhibiting the quantum-well with quantum-confined Stark effect (QCSE)[6], a monolayer of graphene possesses a much stronger interband optical transition, which finds applications in novel optoelectronic devices such as photodetectors[16,17]. (2) Broadband operation. As the high frequency dynamic conductivity for Dirac fermions is constant, the optical absorption of graphene is independent of wavelength, covering all telecommunications bandwidth and also the mid- and far-infrared[18,19]. (3) High-speed operation. With a carrier mobility exceeding 200,000 cm^2 V^{-1} s^{-1} at room temperature[20,21] (this is among the highest known), the Fermi level and hence the optical absorptions of graphene can be rapidly modulated through the band-filling effect. In addition, speed limiting processes in graphene (such as photocarrier generation and relaxation) operate on the timescale of picoseconds[22], which implies that graphene-based electronics may have the potential to operate at 500 GHz, depending on the carrier density and graphene quality. (4) Compatibility with CMOS processing. The athermal optoelectronic properties of graphene and its CMOS-compatible integration processes at wafer scale[23–25] make it a promising candidate for post-CMOS electronics, particularly for high frequency applications. With all these advantages, monolithic integration of a graphene electroabsorption modulator could open new routes to integrated photonics, with a compact footprint, low voltage operation and ultrafast modulation across a broad range of wavelengths.

Here we report the first waveguide-integrated graphene-based electroabsorption modulator, in which modulation is achieved by actively tuning the Fermi level of a monolayer graphene sheet. The gigahertz graphene modulator demonstrates a strong electroabsorption modulation of 0.1 dB μm^{-1} and operates over a broad range of wavelength, from 1.35 μm to 1.6 μm, under ambient conditions.

The structure of the electroabsorption modulator is schematically illustrated in Fig. 1. A 50-nm-thick Si layer was used to connect the 250-nm-thick Si bus waveguide and one of the gold electrodes. Both the silicon layer and the waveguide were shallowly doped with boron to reduce the sheet resistance. A spacer of 7-nm-thick Al$_2$O$_3$ was then uniformly deposited on the surface of the waveguide by atom layer deposition. A graphene sheet grown by chemical vapour deposition[23,24,26] (CVD) was then mechanically transferred onto the Si waveguide. To further reduce the access resistance of the device, the counter electrode was extended towards the bus waveguide by depositing a platinum (10 nm) film on top of the graphene layer. The minimum distance between platinum electrode and waveguide was controlled at 500 nm, so that the optical modes of the waveguide remained undisturbed by the platinum contact. The excess graphene was removed by oxygen plasma, leaving only the regions on top of the waveguide and between the waveguide and the platinum electrode.

The cross-sectional view of the device structure and the optical field distribution of the guided mode are shown in Fig. 1b. The thin silicon layer and the platinum electrode adjacent to the waveguide have negligible effect on the mode profile. To further improve the electroabsorption modulation efficiency, the silicon waveguide was designed to have the electric field maximized at its top and bottom surfaces, so that the interband transitions in graphene are also maximized (Fig. 1b). As

[1]NSF Nano-scale Science and Engineering Center (NSEC), 3112 Etcheverry Hall, University of California at Berkeley, Berkeley, California 94720, USA. [2]Department of Physics, University of California at Berkeley, Berkeley, California 94720, USA. [3]Materials Sciences Division, Lawrence Berkeley National Laboratory, 1 Cyclotron Road, Berkeley, California 94720, USA.
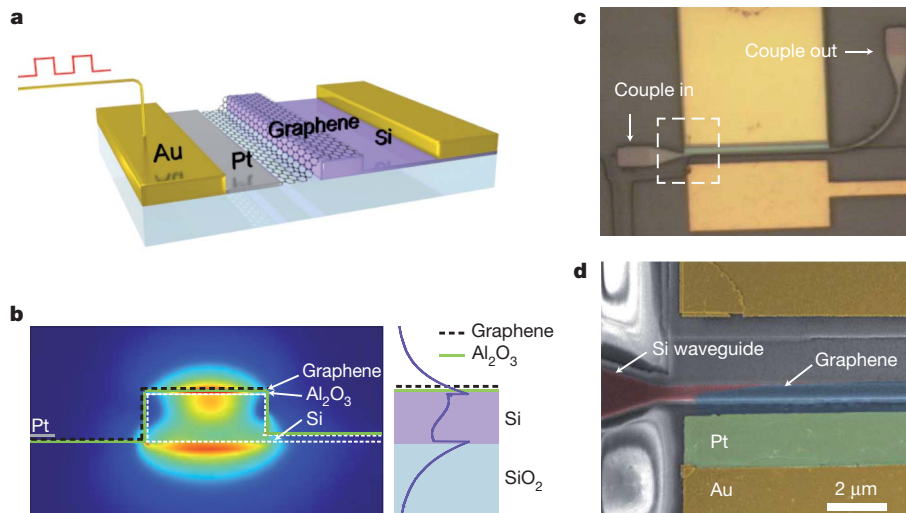*These authors contributed equally to this work.

Figure 1 | A graphene-based waveguide-integrated optical modulator.
a, Three-dimensional schematic illustration of the device; a monolayer graphene sheet is on top of a silicon bus waveguide, separated from it by a 7-nm-thick Al_2O_3 layer (not shown). The silicon waveguide is doped, and connected to the electrode (right, shown gold) through a thin layer of silicon defined by selective etching. **b**, Left, cross-section of the device, with an overlay of the optical mode plot, calculated by finite element simulation. The waveguide was carrying a single optical mode, and was designed so as to maximize the field at the interface between the waveguide and the graphene, to maximize the absorption efficiency. The thin silicon layer and the Pt electrode, which is 500 nm away from the waveguide, have negligible influence on the optical mode. Right, a cross-section through the centre of the waveguide; the purple

curve shows the magnitude of the electric field. The actual thicknesses of the graphene sheet and the Al_2O_3 in the simulation are 0.7 nm and 7 nm, respectively. **c**, Top-view optical microscope image of the waveguide. The Si waveguide was bent by 90° to change the polarization state between the input and the output light, to improve the signal-noise ratio. **d**, SEM image showing the boxed region in **c** at higher magnification, showing the detailed structure of the graphene modulator. False colours are used to highlight the Au electrode (yellow), the Pt electrode (Green), the graphene sheet (blue) and the waveguide (red). The width of the Si waveguide is 600 nm, while the distance between the Pt electrode and the Si waveguide is 500 nm. The bright multi-ring region beside the Au electrodes is due to a charging effect on the SiO_2 layer in the SEM.

graphene only interacts with the tangential (in-plane) electric field of electromagnetic waves, the graphene modulator is polarization-sensitive, as are conventional semiconductor-based electro-optical modulators[3].

Figure 1c shows a top-view optical microscope image of the device, and a close-up scanning electron microscopy image of the active region is given in Fig. 1d. The graphene sheet, highlighted in Fig. 1d by a false blue colour, covers only the waveguide region; this is to minimize the capacitance. The platinum electrode (green) is placed 500 nm away from the 600-nm-wide Si waveguide. Light was coupled in and out of the waveguide through tapered gratings, which contribute most to the overall loss of the system. The Si waveguide was bent 90° to change the polarization state between the input and the output light, to improve the signal-noise ratio.

Figure 2 displays the transmission of 1.53 μm photons through the waveguide at different drive voltages, V_D. At low drive voltage ($-1\,V < V_D < 3.8\,V$), the Fermi level $E_F(V_D)$ of graphene is close to the Dirac point ($E_F(V_D) < h\nu_0/2$), and interband transitions occur when electrons are excited by the incoming photons ($h\nu_0$). The optical absorption of graphene is determined by the position of the Fermi level. By applying a drive voltage between the graphene and the waveguide, we can tune the Fermi level of the graphene, and therefore modulate the total transmission. With the current waveguide design, the modulation depth is as high as 0.1 dB μm^{-1}, resulting in a graphene electroabsorption modulator with a footprint of merely 25 μm^2. At large negative V_D ($<-1\,V$), the Fermi level is lowered below the transition threshold ($E_F(V_D) = h\nu_0/2$) owing to positive charge accumulation. As a result, there are no electrons available for interband transitions, and hence the graphene appears transparent. On the other hand, at large positive V_D ($>3.8\,V$), all electron states are filled up, and no interband transitions are allowed. Ideally, there should be a sharp change in transmission at $E_F(V_D) = h\nu_0/2$. In reality, this transition was broadened owing to defects in the graphene, and shifted to higher voltage owing to natural doping from the substrate[27]. When the modulator is in operation (that is, when no interband absorption is allowed),

its insertion loss is negligible as the intraband absorption of graphene is extremely low at near-infrared wavelengths[28].

To measure the dynamic response of the graphene modulator, radio frequency signals generated by a network analyser were added on a static V_D and applied to the modulator. The same 1.53-μm laser was used to test the modulator, and the out-coupled light was sent to a high-speed photodetector. Shown in Fig. 3 are the V_D-dependent r.f. responses of the graphene modulator; gigahertz operation of the device
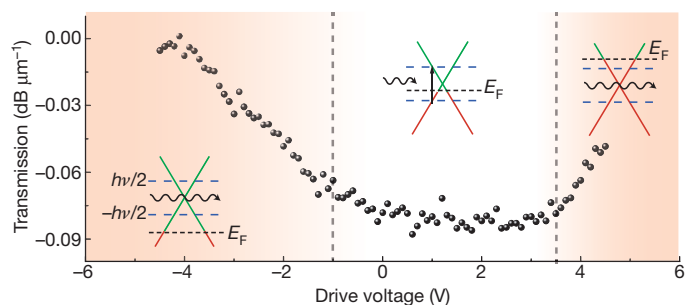

Figure 2 | Static electro-optical response of the device at different drive voltages. The main panel shows the modulation depth, normalized to the device length (40 μm), at different drive voltages (V_D). Three regions can be seen, and their band structures are shown as insets. In the middle region (with V_D in the range $-1\,V$ to 3.8 V), the Fermi level (E_F, black dashed line) is close to the Dirac point and the interband transition is allowed from electron-occupied regions (red lines) to unoccupied regions (green lines). Thus the graphene sheet is absorptive to incident photons ($h\nu$), resulting in a modulation depth of 0.1 dB μm^{-1} and a miniaturized footprint of the modulator. In the left-hand region (with $V_D < -1\,V$), the Fermi level (E_F) is lower than half the photon energy ($-h\nu/2$, blue dashed line) and there are no electrons available for the interband transition. In the right-hand region (with $V_D > 3.8\,V$), all electron states in resonance with incident photons ($h\nu$) are occupied, and the transition is forbidden. In both of the last two cases, the transmission increases. The natural doping from the substrate offsets the centre of the absorption curve from zero bias. The transmission is measured at a laser wavelength of 1.53 μm.
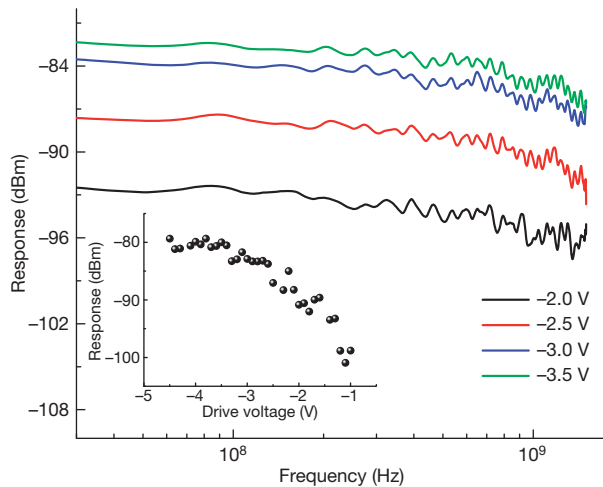
Figure 3 | Dynamic electro-optical response of the device. The main panel shows the response of the device as a function of frequency. Each curve corresponds to a different drive voltage: $-2.0\,\text{V}$, $-2.5\,\text{V}$, $-3.0\,\text{V}$ and $-3.5\,\text{V}$ (black, red, blue and green curve, respectively). The measured 3 dB bandwidths of the device are respectively 0.8 GHz, 1.1 GHz, 1.1 GHz and 1.2 GHz; the bandwidths are mainly restricted by the parasitic response of the device. Inset, low-frequency device response with different drive voltages, indicating that the device has best performance at a drive voltage of $-4\,\text{V}$. The laser wavelength is 1.53 µm in the test.

at various drive voltages is obtained. Owing to the exceptionally high carrier mobility and saturation velocity of graphene, the bandwidth is not limited by the carrier transit time, but by the parasitic response of the device. With the platinum electrode placed 500 nm away from the waveguide, the total resistance of the system is reduced to around 600 Ω. This resistance, together with the capacitance (of the order of 0.22 pF), limits the operation bandwidth of the present device to about 1 GHz (see Fig. 3 legend).

The device response at low frequency (300 kHz) is shown in Fig. 3 inset. At low V_D, the modulation response is weak, as the optical transmission is insensitive to V_D. When the drive voltage is increased, the r.f. response increases to a maximum at $V_D = -4\,\text{V}$. As the drive voltage increases further, the modulation efficiency saturates, as graphene is then transparent within the modulation range of the bias voltage.

As the overall optical opacity of graphene is independent of wavelength and the high frequency dynamic conductivity for Dirac fermions is constant, the graphene electroabsorption modulator is therefore intrinsically broadband, unlike modulators that are based on optical cavities or resonant optical effects (such as QCSE). In order to investigate this broadband effect, we study the static response of the device to a white light source from a supercontinuous laser. The response is shown as a function of wavelength and V_D in Fig. 4a; we refer to this as a two-dimensional (2D) transmission spectrum. A 3 dB modulation, corresponding to a transmission value of 2 (a.u.) in Fig. 4a, is achieved for a broad band of wavelengths, from 1.35 µm to 1.6 µm. Although a higher modulation depth and broader wavelength range are expected at a higher drive voltage, we chose to use low drive voltage not only to avoid spacer oxide breakdown but also because high drive voltages increase power consumption and violate voltage restrictions in CMOS devices.

Two-dimensional transmission spectra also allow us to determine the electronic band dispersion of the graphene. As the graphene electroabsorption modulation is dictated by the optical transition, $h\nu = 2E_F$, the graphene modulator has a different response at different wavelengths. Operation at higher photon energy ($h\nu$) always requires a larger change in the Fermi level (E_F). The trace of critical drive voltage (V) for maximum transmission change rate, shown as a dashed line in Fig. 4a, is defined by $h\nu = 2E_F = 2\hbar\nu_F\sqrt{\eta\pi|V + V_0|}$, where ν_F is the Fermi velocity, V_0 is the voltage offset caused by natural doping, and
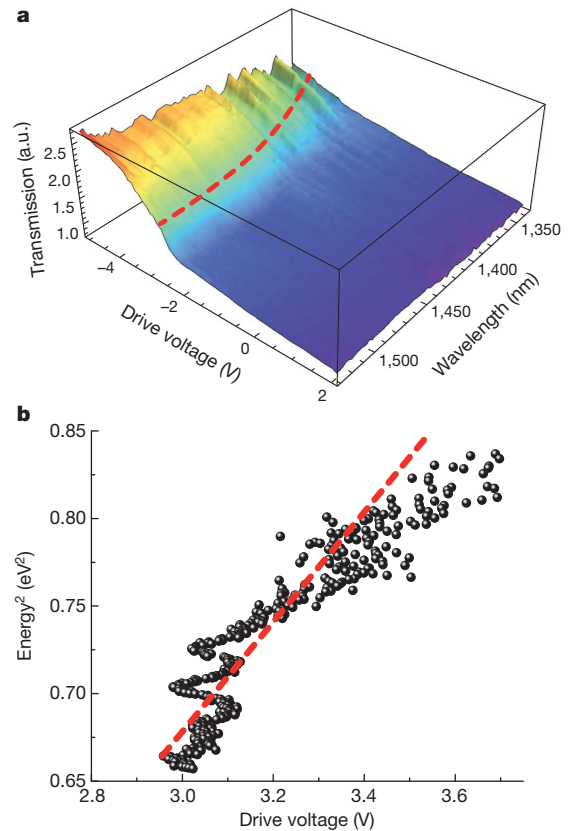

Figure 4 | Spectrum characterization of the optical modulator. a, The transmission of the device as a function of drive voltage and wavelength (1,350–1,600 nm). The transmission is normalized to $V_D = 1\,\text{V}$. The red dashed curve shows the trace for maximum transmission change rate, which unambiguously bends to higher drive voltages at shorter wavelengths. **b**, Squared photon energy versus critical drive voltage for maximum transmission change rate. The red dashed line shows a linear fit to the experimental data, which directly yields the Fermi velocity of $\nu_F = 0.9 \times 10^6\,\text{m s}^{-1}$.

$\eta = 9 \times 10^{16}\,\text{m}^{-2}\,\text{V}^{-1}$, as estimated using a parallel-plate capacitor model of our device. The relation between critical drive voltage and the square of the photon energy is plotted in Fig. 4b. The linear fit (red dashed line) yields the voltage offset ($-0.8\,\text{V}$) and the Fermi velocity ($0.9 \times 10^6\,\text{m s}^{-1}$), which agree with other reported values[29].

We have demonstrated a graphene-based optical modulator that has broad optical bandwidth (1.35–1.6 µm), small device footprint (25 µm^2) and high operation speed (1.2 GHz at 3 dB) under ambient conditions, all of which are essential for optical interconnects for future integrated optoelectronic systems. The modulation efficiency of a single layer of carbon atoms in a hexagonal lattice (graphene) is already comparable to, if not better than, traditional semiconductor materials such as Si, GeSi and InGaAs, which are orders of magnitude larger in active volume. The flexibility of graphene sheets could also enable radically different photonic devices. For example, graphene could be integrated with flexible substrate and plastic waveguides[30]. Or it could be used in novel geometries, such as a flexible modulator on a nano-optical cable. The recent development of large scale graphene synthesis and transfer techniques[23] ensure its compatibility with the existing integrated electronics platform.

1. Miller, D. A. B. Are optical transistors the logical next step? *Nature Photon.* **4,** 3–5 (2010).
2. Reed, G. T., Mashanovich, G., Gardes, F. Y. & Thomson, D. J. Silicon optical modulators. *Nature Photon.* **4,** 518–526 (2010).
3. Liu, A. S. *et al.* A high-speed silicon optical modulator based on a metal-oxide-semiconductor capacitor. *Nature* **427,** 615–618 (2004).

4. Kuo, Y. H. *et al.* Strong quantum-confined Stark effect in germanium quantum-well structures on silicon. *Nature* **437,** 1334–1336 (2005).

5. Liu, J. *et al.* Waveguide-integrated, ultralow-energy GeSi electro-absorption modulators. *Nature Photon.* **2,** 433–437 (2008).

6. Miller, D. A. B. *et al.* Band-edge electroabsorption in quantum well structures — the quantum-confined Stark-effect. *Phys. Rev. Lett.* **53,** 2173–2176 (1984).

7. Xu, Q., Schmidt, B., Pradhan, S. & Lipson, M. Micrometre-scale silicon electro-optic modulator. *Nature* **435,** 325–327 (2005).

8. Novoselov, K. S. Electric field effect in atomically thin carbon films. *Science* **306,** 666–669 (2004).

9. Geim, A. K. & Novoselov, K. S. The rise of graphene. *Nature Mater.* **6,** 183–191 (2007).

10. Schwierz, F. Graphene transistors. *Nature Nanotechnol.* **5,** 487–496 (2010).

11. Bonaccorso, F., Sun, Z., Hasan, T. & Ferrari, A. Graphene photonics and optoelectronics. *Nature Photon.* **4,** 611–622 (2010).

12. Liao, L. *et al.* High-speed graphene transistors with a self-aligned nanowire gate. *Nature* **467,** 305–308 (2010).

13. Avouris, P., Chen, Z. H. & Perebeinos, V. Carbon-based electronics. *Nature Nanotechnol.* **2,** 605–615 (2007).

14. Wang, F. *et al.* Gate-variable optical transitions in graphene. *Science* **320,** 206–209 (2008).

15. Li, Z. Q. *et al.* Dirac charge dynamics in graphene by infrared spectroscopy. *Nature Phys.* **4,** 532–535 (2008).

16. Xia, F. N., Mueller, T., Lin, Y. M., Valdes-Garcia, A. & Avouris, P. Ultrafast graphene photodetector. *Nature Nanotechnol.* **4,** 839–843 (2009).

17. Xu, X., Gabor, N. M., Alden, J. S., van der Zande, A. M. & McEuen, P. L. Photo-thermoelectric effect at a graphene interface junction. *Nano Lett.* **10,** 562–566 (2010).

18. Nair, R. R. *et al.* Fine structure constant defines visual transparency of graphene. *Science* **320,** 1308 (2008).

19. Mak, K. F. *et al.* Measurement of the optical conductivity of graphene. *Phys. Rev. Lett.* **101,** 196405 (2008).

20. Bolotin, K. I. *et al.* Ultrahigh electron mobility in suspended graphene. *Solid State Commun.* **146,** 351–355 (2008).

21. Du, X., Skachko, I., Barker, A. & Andrei, E. Y. Approaching ballistic transport in suspended graphene. *Nature Nanotechnol.* **3,** 491–495 (2008).

22. Kampfrath, T., Perfetti, L., Schapper, F., Frischkorn, C. & Wolf, M. Strongly coupled optical phonons in the ultrafast dynamics of the electronic energy and current relaxation in graphite. *Phys. Rev. Lett.* **95,** 187403 (2005).

23. Kim, K. S. *et al.* Large-scale pattern growth of graphene films for stretchable transparent electrodes. *Nature* **457,** 706–710 (2009).

24. Bae, S. *et al.* Roll-to-roll production of 30-inch graphene films for transparent electrodes. *Nature Nanotechnol.* **5,** 574–578 (2010).

25. Reina, A. *et al.* Large area, few-layer graphene films on arbitrary substrates by chemical vapor deposition. *Nano Lett.* **9,** 30–35 (2009).

26. Li, X. *et al.* Large-area synthesis of high-quality and uniform graphene films on copper foils. *Science* **324,** 1312–1314 (2009).

27. Zhang, Y. B., Brar, V. W., Girit, C., Zettl, A. & Crommie, M. F. Origin of spatial charge inhomogeneity in graphene. *Nature Phys.* **5,** 722–726 (2009).

28. Jablan, M., Buljan, H. & Soljačić, M. Plasmonics in graphene at infrared frequencies. *Phys. Rev. B* **80,** 245435 (2009).

29. Zhou, S. Y. *et al.* First direct observation of Dirac fermions in graphite. *Nature Phys.* **2,** 595–599 (2006).

30. Rogers, J. A., Someya, T. & Huang, Y. G. Materials and mechanics for stretchable electronics. *Science* **327,** 1603–1607 (2010).

Author Contributions M.L. and X.Z. contributed to the experimental ideas. M.L. fabricated device samples. M.L. and X.Y. carried out measurements, analysed the experimental data and prepared the manuscript. B.G., L.J. and F.W. prepared graphene film. All authors contributed to discussions and manuscript revision.

Author Information Reprints and permissions information is available at www.nature.com/reprints. The authors declare competing financial interests: details accompany the full-text HTML version of the paper at www.nature.com/nature. Readers are welcome to comment on the online version of this article at www.nature.com/nature. Correspondence and requests for materials should be addressed to X.Z. (xiang@berkeley.edu, for general experimental details) and F.W. (fengwang76@berkeley.edu, for details of graphene synthesis).